RSC Advances

PAPER

View Article Online
View Journal | View Issue

Cite this: *RSC Adv.*, 2015, **5**, 50344

Effect of acid-leaching on carbon-supported copper phthalocyanine tetrasulfonic acid tetrasodium salt (CuTSPc/C) for oxygen reduction reaction in alkaline electrolyte: active site studies†

Qing Zhang,[a] Taishan Zhu,[b] Xin Qing,[b] Jinli Qiao*[ab] and Shuhui Sun*[c]

Although non-precious metal catalysts (NPMCs) have been extensively studied as low-cost catalyst alternatives to Pt, in particular for the oxygen reduction reaction (ORR) in polymer electrolyte membrane fuel cells (PEMFCs), the nature of the active ORR catalytic sites is still a subject of controversy. In this work, using carbon-supported copper phthalocyanine tetrasulfonic acid tetrasodium salt (CuTSPc/C) nanoparticles as the target catalyst, the effects of the transition metal Cu on the ORR active sites are systematically studied using both rotating disk electrode (RDE) and rotating ring disk electrode (RRDE) techniques in alkaline electrolyte. The results show that acid-leaching can significantly decrease the ORR activity of the CuTSPc/C catalyst, with the half-wave potential negatively shifted by more than 50 mV compared to the catalyst before acid-leaching. The electron transfer number of the ORR process catalyzed by the catalyst before acid-leaching remained at about 3.85 over the whole tested potential range from −0.6 to −0.1 V, while this number greatly decreased from 3.82 at −0.55 V to 3.53 at −0.1 V after acid-leaching. The H_2O_2 produced accordingly increased sharply from 7.8% to 22%. XRD and TEM results indicate that acid-leaching is an effective method to remove metal-Cu. XPS analysis reveals that metal-Cu is essential in the ORR active site structure, and also plays a key part in the stabilization of the active N and S species.

Received 9th April 2015
Accepted 28th May 2015

DOI: 10.1039/c5ra06314k

www.rsc.org/advances

1. Introduction

Increasing energy demand and environmental pollution have stimulated significant research into new, efficient and sustainable energy sources to compensate for and even replace traditional ones.[1,2] In this regard, proton-exchange membrane (PEM) fuel cells have attracted great attention as a promising green energy device due to them having several advantages, such as high energy efficiency, high energy/power densities, and low/zero emissions.[3–5] To date, the slow cathodic oxygen reduction reaction (ORR) kinetics and large overpotential (or polarization) have been identified as the major barrier in a fuel cell.[6] To make PEM fuel cells technically feasible and practical, in the current state of technology, Pt-based catalysts must be used to catalyze the slow ORR due to their high catalytic performances for both the anode and cathode. However, as Pt-based catalysts have insufficient electrochemical durability and come at a high cost,[6–8] the major efforts in PEM fuel cell research and development have been put into reducing Pt loading by exploring more active catalysts, and/or replacing Pt metal with other, non-precious, metals such as Fe, Co and Cu.[9,10] In spite of current progress, very few examples show real promise to be comparable to Pt since the requirements for both good ORR activity and stability are difficult to achieve for normal non-noble catalysts in the strongly acidic conditions of PEM fuel cell operation.

Recently, the growing interest in the application of alkaline fuel cells (AFCs) has been principally motivated by the prospective use of cheap, easy to use, and relatively abundant non-precious metal catalysts (NPMCs).[11–13] In a basic environment, the catalyst activity toward the ORR is much higher, and greatly improved material stability is afforded, thus leading to reduced Pt loading and extended choices for suitable Pt alternatives.[11–13] In particular, extensive work has been done to develop transition metal N-containing complexes, conductive polymer-based catalysts, transition metal chalcogenides, metaloxides/carbides/nitrides/oxynitrides/carbonitrides and

[a]*School of Chemistry and Chemical Engineering, Key Laboratory of Green Chemical Media and Reactions, Ministry of Education, Henan Normal University, Xinxiang, Henan 453007, P. R. China. E-mail: qiaojl@dhu.edu.cn; shuhui@emt.inrs.ca; Fax: +86-21-67792159; Tel: +86-21-67792379*

[b]*College of Environmental Science and Engineering, Donghua University, 2999 Ren'min North Road, Shanghai 201620, P. R. China*

[c]*Institut National de la Recherche Scientifique (INRS), Energie Materiaux Telecommunications Research Center, 1650 Boul. Lionel-Boulet Varennes, Quebec, J3X 1S2, Canada*

† Electronic supplementary information (ESI) available. See DOI: 10.1039/c5ra06314k

enzymatic compounds.[14–18] Among these NPMCs, pyrolyzed metal–nitrogen materials supported on carbon (M–N_X/C) are considered as the most promising ORR catalysts, especially Fe- and/or Co-based ones.[11,14,19] As yet, the ORR activity of this kind of non-precious metal catalyst is still insufficient. Although some methods and materials have widely been used to produce active non-precious metal ORR catalysts, there are still difficulties in discerning the controlling parameters in preparing active catalysts. There is a general agreement in the literature that the type of transition metal, nitrogen and carbon support and the pyrolysis process all have effects on the ORR activity and stability of a catalyst.[20–23] Among these four factors, the nitrogen and the carbon support are considered to be essential for the active sites. Regarding the role of the metal ion in the catalytic process, however, there are two different views: (i) the presence of metal ions plays an important role in the formation of active sites (M–N_X/C, $X = 2$ or 4);[24–26] (ii) the transition metal does not act as part of the active site, and instead only helps to facilitate the stable incorporation of nitrogen into the graphitic structure of carbon, and the formation of active carbon during high-temperature pyrolysis.[27]

To form N-containing non-precious metal catalysts for the ORR, metal phthalocyanines (MPcs) have been explored as catalyst precursors due to their unique delocalized conjugated bonds with eight N atoms in a unit structure, making MPcs liable to oxidation and reduction.[21,28–32] In particular, the pyrolyzed Co- and Fe-centered phthalocyanines have been proven to be the most promising catalysts, exhibiting remarkable ORR activities close to that of the commercially available Pt/C catalyst.[21,28,29] On the other hand, it has also been found that the ORR activity of MPcs strongly depends on the central metal ions[22,30] and the pH value of the electrolyte.[31] For example, Sehlotho *et al.* found that MnPc complexes could catalyze a 2-electron transfer ORR in acidic media, but a 4-electron transfer ORR in alkaline media.[31] Most recently, we have demonstrated the excellent ORR activity of carbon-supported copper phthalocyanine (CuPc), which even surpasses pyrolyzed CoPc/C in alkaline condition.[32] In a continuing effort, we further report that metal-Cu, nitrogen and sulfur can be simultaneously formed onto the carbon support framework to form new Cu–N–S/C catalysts by pyrolyzing a carbon-supported copper phthalocyanine tetrasulfonic acid tetrasodium salt (CuTSPc/C) nanoparticle catalyst, without additional dopant precursor.[33] As shown in Table 1, in the use of EDX-mapping data for exploring the active site structure, an interesting phenomenon can be seen: the nitrogen content in the catalysts shows no significant decline with an increase in heat-treatment temperature. This suggests that the presence of Cu and S species could prevent phthalocyanine from undergoing thermal decomposition and contribute to a higher nitrogen content during the pyrolysis process (where a greater nitrogen concentration in the synthesis of the catalyst could benefit the ORR activity of the catalyst). Moreover, S has also been proven to be an essential part of the ORR active site, and the synergetic effect between N and S could be spontaneously formed within the catalyst.[33] Nevertheless, the role of the transition metal in the active sites of the catalysts is still unclear.

Table 1 The elemental compositions for CuTSPc/C synthesized at different temperatures, determined by EDS

	CuTSPc/C		(CuTSPc/C)$_{600}$		(CuTSPc/C)$_{700}$		(CuTSPc/C)$_{800}$	
Element	Wt%	At%	Wt%	At%	Wt%	At%	Wt%	At%
C	64.88	72.71	66.96	74.27	67.72	74.33	80.90	86.05
N	11.11	10.67	12.11	11.52	11.84	11.14	9.26	8.45
O	15.32	12.89	13.09	10.90	14.86	12.24	4.86	3.88
Na	3.00	1.75	3.01	1.75	1.86	1.07	0.24	0.13
S	3.69	1.55	2.71	1.13	2.20	0.91	2.75	1.10
Cu	2.00	0.42	2.11	0.44	1.52	0.31	1.99	0.40

Inspired by the results achieved in our continuing effort, in this work, with carbon-supported copper phthalocyanine tetrasulfonic acid tetrasodium salt (CuTSPc/C) nanoparticles as the target catalyst, the role of the central metal-Cu ion in the macrocycle complex was investigated using an acid-leaching model. The catalytic ORR activities of the catalysts before and after acid-leaching were studied thoroughly using linear sweep voltammetry (LSV), employing rotating disk electrode (RDE) and rotating ring-disk electrode (RRDE) techniques in 0.1 M KOH. The ORR kinetic parameters and the possible reaction mechanisms are discussed. For fundamental understanding, XRD, TEM and XPS analyses were also performed to identify the surface structure change and the possible active sites of these catalysts before and after acid-leaching.

2. Experimental

2.1. Materials and catalyst preparation

Copper phthalocyanine tetrasulfonic acid tetrasodium salt (CuTSPc) was provided by Sigma Aldrich with 60% purity and was used as both the metal precursor and nitrogen precursor. In this work, Vulcan XC-72R carbon black was used as the carbon support, which was purchased from Cabot Corporation with 236.8 $m^2\ g^{-1}$ specific surface area. Carbon-supported copper phthalocyanine tetrasulfonic acid tetrasodium salt catalysts (CuTSPc/C) were prepared *via* a combined solvent-impregnation and milling procedure along with high-temperature treatment. In detail, the preparation was carried out by combining a mixture of 40 mg CuTSPc and 60 mg carbon black in a mortar, milling by adding 10 ml methanol for 2 h, and then vacuum-drying at 40 °C for 1 h to remove the methanol. The resulting catalyst was placed in a quartz boat and pyrolyzed at 700 °C for 120 min at a rate of 20 °C min^{-1} in a flowing nitrogen atmosphere. This as-prepared catalyst is designated as (CuTSPc/C)$_{700}$. In order to remove the metal-Cu, the catalyst was subjected to an acid-leaching procedure after heat-treatment. In detail, the (CuTSPc/C)$_{700}$ catalyst was refluxed in 0.5 M H_2SO_4 at 80 °C for 8 h, then the suspension was washed with deionized (D.I.) water and centrifuged until the supernatant was neutral. The obtained catalyst powder was finally dried at 60 °C in an oven overnight under ambient air conditions, and was then designated as (CuTSPc/C)$_{700}$AL.

2.2. Physical characterizations

The microstructures of both $(CuTSPc/C)_{700}$ and $(CuTSPc/C)_{700}AL$ catalysts were examined using X-ray powder diffraction (XRD), transmission electron microscopy (TEM) and X-ray photoelectron spectroscopy (XPS). XRD measurements were carried out on a Philips PW3830 X-ray diffractometer equipped with Cu-Kα radiation ($\lambda = 0.15406$ nm). The current was 40 mA and the voltage was 40 kV. The intensity data were collected at 25 °C in the 2θ range from 0° to 90° with a scan rate of 1.20° min^{-1}. TEM was performed on a JEM-2100F operated at an acceleration voltage of 200 kV to obtain information on the average particle size and distribution of the prepared catalyst. XPS analysis was carried out on a Kratos AXIS $Ultra^{DLD}$ electron spectrometer with an Al K X-ray anode source ($h\nu = 1486.6$ eV) at 250 W and 14.0 kV. The XPS Peak 41 software was used for fitting the XPS spectrum.

2.3. Electrochemical measurements

All the electrochemical measurements were carried out in a conventional three-electrode cell using a CHI760D electrochemical workstation controlled at room temperature. The electrocatalytic activities of both $(CuTSPc/C)_{700}$ and $(CuTSPc/C)_{700}AL$ catalysts were evaluated using linear sweep voltammetry (LSV) with rotating disk electrode (RDE) and rotating ring-disk electrode (RRDE) techniques. A glassy carbon (GC) electrode (with a diameter of 5.615 mm corresponding to a geometric surface area of 0.2475 cm^2, purchased from Pine Instruments) was used as the working electrode. Prior to use, the GC electrode surface was polished with Al_2O_3 (0.05 μm) suspension and rinsed with D.I. water. The catalyst ink was prepared by mixing 25 mg of the catalyst with 2 ml of isopropyl alcohol to form a mixture, which was then ultrasonically dispersed for 45 minutes to dissolve the catalyst as evenly as possible. Then 10 μl of the catalyst ink was deposited onto the GC electrode surface, leading to a catalyst loading of 0.5 mg cm^{-2}. After drying at room temperature, one drop of methanol–Nafion® solution (50 : 1 wt%) was dropped onto the top of the catalyst layer to improve adhesion during the electrochemical measurement.

RDE experiments were performed in a three-electrode electrochemical cell at room temperature, and 0.1 M KOH was used as the electrolyte. A saturated calomel electrode (SCE) and platinum wire were used as the reference and counter electrodes, respectively. All measured potentials were referenced to a standard hydrogen electrode (SHE). Linear sweep voltammetry (LSV) in O_2-saturated 0.1 M KOH was carried out at 1500 rpm with a sweep rate of 5 mV s^{-1} and a potential range between −0.6 and 0.3 V. To verify the ORR catalytic pathways of the catalyst, RRDE measurements were performed to monitor the formation of peroxide species during the ORR process.

3. Results and discussion

3.1. Oxygen reduction reaction activity

According to the literature, "metal-free" catalysts are normally considered to exhibit better stability than transition metal N-containing complexes because there are no issues related to metal dissolution and poisoning, as observed with metal-containing catalysts,[34–36] and acid-leaching (heating with H_2SO_4) is usually used for removing the transition metal ions during catalyst synthesis.[37,38] However, there has been no report on the use of acid-leaching for the pyrolyzed macrocyclic structured metal phthalocyanines. Fig. 1 shows the ORR polarization curves of the CuTSPc/C catalyst electrode before and after acid-leaching, measured in O_2-saturated 0.1 M KOH at room temperature. One can see that the $(CuTSPc/C)_{700}$ catalyst gives an onset potential of 0.18 V and a half-wave potential ($\Delta E_{1/2}$) of 0.04 V, along with a better-defined diffusion-limiting current plateau ranging from −0.2 to −0.6 V. This suggests that the distribution of active sites on the $(CuTSPc/C)_{700}$ electrode is uniform and the oxygen reduction reaction rate is fast enough. On the contrary, compared to the $(CuTSPc/C)_{700}$ catalyst, the $(CuTSPc/C)_{700}AL$ catalyst exhibited an onset potential of 0.13 V with a half-wave potential ($\Delta E_{1/2}$) of 0.00 V, *i.e.*, after acid-leaching the electrocatalytic activity of the catalyst decreased greatly, with the half-wave potential of $(CuTSPc/C)_{700}AL$ being negatively shifted by more than 50 mV compared to $(CuTSPc/C)_{700}$. In addition, the good current plateau observed for the $(CuTSPc/C)_{700}$ electrode was also destroyed to some extent, particular in the high-polarization range. The above results indicate that the acid-leaching procedure has a negative effect on the ORR activity. Since the aim of acid-leaching in this work is to remove the central metal-Cu, it can be concluded that the presence of metal-Cu might be beneficial for promoting more oxygen reduction active sites in the $(CuTSPc/C)_{700}$ catalyst, as will be discussed below.

For a further comparison of the catalytic ORR activity of the CuTSPc/C catalyst before and after acid-leaching, the mass-corrected Tafel plots of $\log j_k$ (mA cm^{-2}) *vs.* the electrode potential E are constructed in Fig. 1(b), for both $(CuTSPc/C)_{700}$ and $(CuTSPc/C)_{700}AL$ electrodes. These Tafel curves were deduced from the polarization curves of Fig. 1(a) with a rotation rate of 1500 rpm. It can be clearly seen that the Tafel slopes for the $(CuTSPc/C)_{700}$ catalyst can be divided into two parts, *i.e.*, about 77.6 mV dec^{-1} in the lower overpotential region ($E < 150$ mV *vs.* SHE) and about 127.8 mV dec^{-1} in the higher overpotential region ($E < 50$ mV *vs.* SHE), implying that a 1-electron process is involved in the rate-determining step.[24] On the contrary, the Tafel slope of the $(CuTSPc/C)_{700}AL$ catalyst is high above 185.7 mV dec^{-1} in the higher overpotential region, where $E < -50$ mV *vs.* SHE. These data clearly indicate that the ORR mechanism strongly depends on the electrode materials (*i.e.*, the acid-leaching process) investigated in this work, as also evidenced by the different number of electrons involved in the ORR.

It is known that the electrochemical reduction of oxygen is a multi-electron reaction that has two main possible pathways: one involving gain of $2e^-$ to produce H_2O_2, and the other, a direct $4e^-$ pathway to produce water. In PEMFC operation, the favoured ORR process is expected to be a 4-electron transfer process from O_2 to H_2O rather than to H_2O_2 in order to obtain the maximum energy capacity. Therefore, for further understanding of the catalytic performance of the $(CuTSPc/C)_{700}$

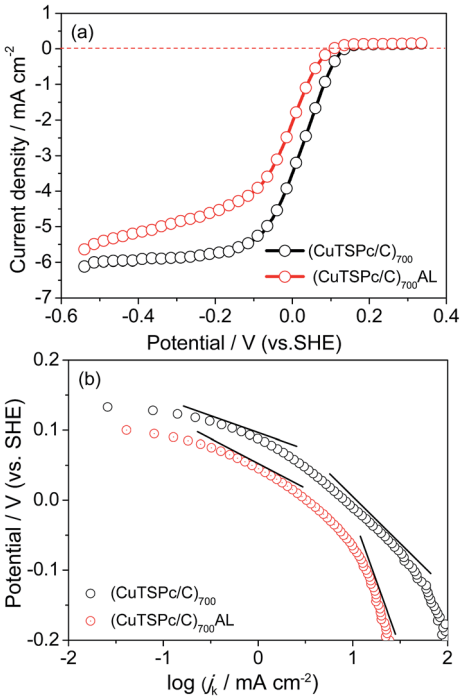

Fig. 1 (a) Polarization curves of ORR catalyzed by $(CuTSPc/C)_{700}$ and $(CuTSPc/C)_{700}AL$ catalysts in O_2-saturated 0.1 M KOH solution. (b) Tafel plots of log j_k *vs.* E (V) for ORR catalyzed by $(CuTSPc/C)_{700}$ and $(CuTSPc/C)_{700}AL$ catalysts, deduced from the polarization curves in (a). Scan rate: 5 mV s^{-1}. Electrode rotation rate: 1500 rpm. Catalyst loading: 505 μg cm^{-2}.

catalyst in the absence of Cu, the RRDE measurements were used to quantitatively verify the ORR catalytic pathway of the catalyst after acid-leaching. Based on the RRDE measurements in Fig. 2(a) and (b), the number of electrons transferred (n) and the percentage of H_2O_2 produced can be calculated according to the formulas:[26]

$$n = \frac{4I_d}{I_d + I_r/N} \quad (1)$$

$$\%H_2O_2 = 100 \times \frac{2I_r/N}{I_d + I_r/N} \quad (2)$$

where I_d, I_r and N are the disk current, ring current, and collection efficiency (0.37 in the present work), respectively. According to these equations, we can calculate the percentage of peroxide species and the number of electrons transferred as shown in Fig. 2(c) and (d). It can be seen that $(CuTSPc/C)_{700}$ and $(CuTSPc/C)_{700}AL$ could both catalyze the ORR with a 4-electron transfer-dominated process. Nevertheless, the electron transfer number of the ORR process catalyzed by $(CuTSPc/C)_{700}$ (*i.e.*, before acid-leaching) remained at about 3.85 over the whole tested potential range from −0.6 to −0.1 V, whereas this number decreased greatly from 3.82 at −0.55 V to 3.53 at −0.1 V for $(CuTSPc/C)_{700}AL$ (*i.e.*, after acid-leaching). The H_2O_2 produced for the latter thus increased sharply from 7.8% to 22%. In fact, the variability of these two kinetic parameters (n and $\%H_2O_2$) is much larger for the catalyst after acid-leaching than before acid-leaching. Obviously, the results in Fig. 2 indicate that the presence of metal-Cu may not only influence the ORR path, but also may have a certain effect on the catalytic stability.

3.2. Morphology and structural characterizations

Fig. 3 shows the XRD patterns for both $(CuTSPc/C)_{700}$ and $(CuTSPc/C)_{700}AL$ in order to clarify the structure change before and after acid-leaching, which can help us to have a further understanding of the mechanisms of influence of acid-leaching on the ORR activity. For both samples, two large broad peaks located at $2\theta = 24.5°$ and $2\theta = 43.0°$ are assigned to the (002) and (100) reflections of the amorphous carbon support (Vulcan XC-72R).[39,40] From Fig. 3(a), it is noted that the reflections which would be characteristic for copper particles are not present; instead, the $(CuTSPc/C)_{700}$ catalyst sample shows two better resolved characteristic peaks of a sulfated copper(I)-containing compound $(NaCu_2(SO_4)_2OH \cdot H_2O)$ at $2\theta = 31.9°$ (ref. 41) and copper hydroxide $(Cu(OH)_2)$ at $2\theta = 34.0°$.[42] Also, the reflection around $2\theta < 10°$, which is associated with the crystalline nature of CuTSPc, was not observed. These results imply that the macrocyclic structure of CuTSPc decomposes when the pyrolysis temperature exceeds 700 °C, resulting in the rearrangement of the carbon and nitrogen atoms. However, a large amount of Cu atoms are in the form of a Cu–N–S/C structure (which is considered to be the oxygen reduction active site)[33] or compounds other than metallic Cu (which are not active for the ORR) (Fig. 3(a)). Very differently from the $(CuTSPc/C)_{700}$ catalyst sample, the above copper-containing characteristic peaks completely disappeared for $(CuTSPc/C)_{700}AL$, as can be clearly seen in Fig. 3(b), indicating that the metal-Cu may be removed after acid-leaching. Based on the electrochemical measurement results (Fig. 1 and 2), this may explain the fact that why we observed higher ORR activity of $(CuTSPc/C)_{700}$ catalyst than that of $(CuTSPc/C)_{700}AL$ catalyst. Combining what will be discussed later, the presence of the metal-Cu might has a great effect on the formation of ORR active site structures as will be further verified by the following TEM analysis.

Fig. 4 shows the typical TEM images for both catalyst samples, which can help us to understand the morphology and particle size differences before and after acid-leaching. It can be seen that for the $(CuTSPc/C)_{700}$ catalyst (Fig. 4(a)), bright particles with sizes of about 20–30 nm are uniformly distributed on the surface of the carbon support. The shape of these particles can also be seen in Fig. 4(b), an enlargement of the area outlined in Fig. 4(a). More interestingly, Fig. 4(b) clearly shows a lattice fringe spacing of 1.25 nm, corresponding to the lattice images of the single-crystal copper (002) plane,[43] which has never been reported in the literature for pyrolyzed metal phthalocyanines. These particles are the Cu-containing cluster compound (Cu–N–S/C), which is considered to be a highly catalytic active for the ORR, as has been reported in our recent work.[33] In the case of the $(CuTSPc/C)_{700}AL$ catalyst (Fig. 4(c)), however, the TEM image surface only shows agglomerated carbon carrier, and no Cu-containing particles with crystal structure can be found. Based on the above-mentioned results,

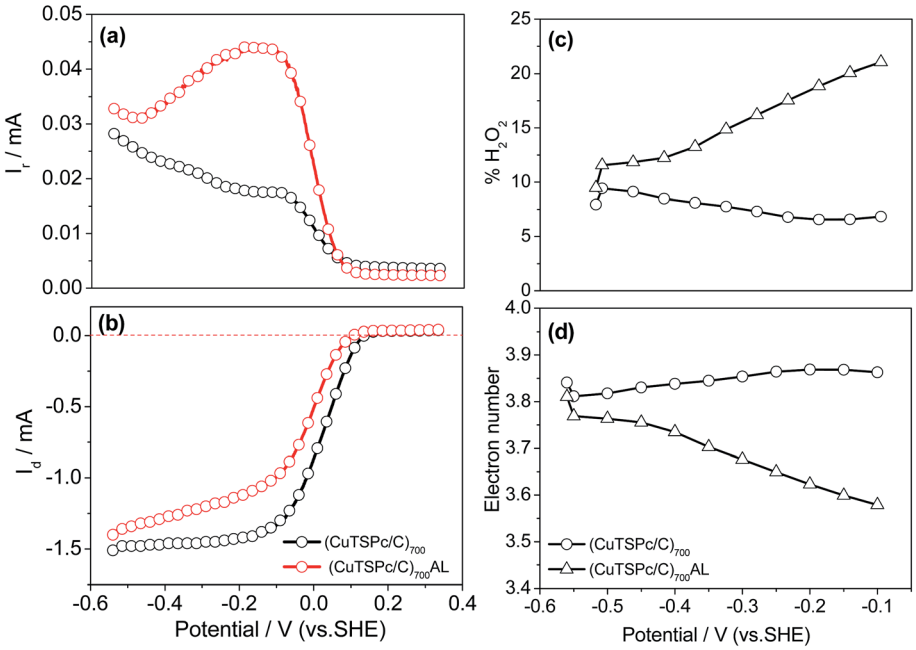

Fig. 2 (a) Rotating ring-disk electrode measurements for ORR catalyzed by $(CuTSPc/C)_{700}$ catalysts synthesized before and after acid-leaching at a scan rate of 5 mV s^{-1} in O_2-saturated 0.1 M KOH solution, (b) the same as Fig. 1, (c) the corresponding $\%H_2O_2$ yield, and (d) electron transfer number of ORR catalyzed by the indicated sample. Catalyst loading: 505 μg cm^{-2}. Rotation rate: 1500 rpm.

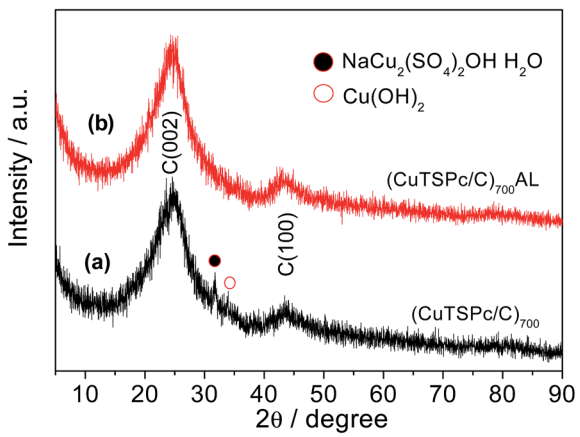

Fig. 3 X-ray diffraction pattern of (a) $(CuTSPc/C)_{700}$ and (b) $(CuTSPc/C)_{700}AL$ catalysts.

it is clear that the structure of Cu–N–S/C was destroyed due to loss of Cu after acid-leaching, which is in good agreement with what we have observed from the XRD results (Fig. 3).

3.3. Active site studies

To further clarify the possible active sites for the ORR catalyzed by the $(CuTSPc/C)_{700}$ catalysts before and after acid-leaching, XPS analyses are carried out and the results are summarized in Fig. 5. In the full-spectrum analysis, the emissions from the C1s, N1s, O1s and S2p levels that constitute the molecules for both $(CuTSPc/C)_{700}$ and $(CuTSPc/C)_{700}AL$ were clearly observed. The Cu that is present in the molecules of $(CuTSPc/C)_{700}$ was also clearly identified (XPS; see Fig. S1, ESI†). However, the peaks of Cu2p were not found after acid-leaching, and the content of Cu is too small to be detected. This can be seen more intuitively in Table 2. As seen more clearly in Fig. 5(a), the Cu2p spectrum for the $(CuTSPc/C)_{700}$ catalyst sample can be deconvoluted into four peaks, except for the higher energy band of the Cu2p spectrum which originates from a broad Cu(II) satellite extending from 940 to 950 eV. The four narrow peaks at 932.4, 933.4, 934.5 and 935.4 eV are ascribed to cuprous species,[43–45] copper nitrides,[46] copper hydroxide[47,48] and part of the undecomposed CuTSPc/C, respectively. Although the peak at 935.4 eV can still be observed, both peak height and peak area

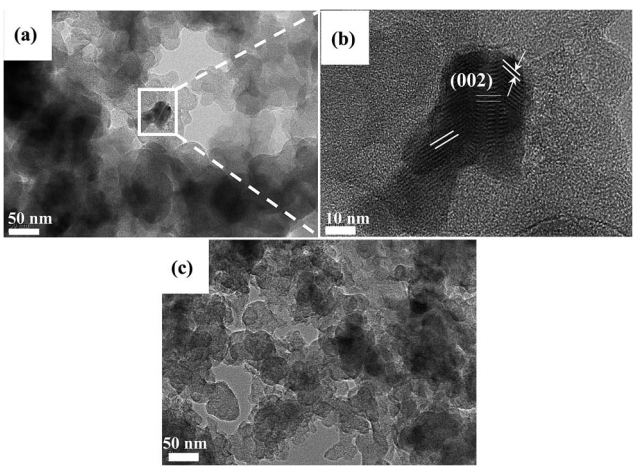

Fig. 4 TEM images of (a) $(CuTSPc/C)_{700}$, (b) an enlargement of the area outlined in (a), and (c) $(CuTSPc/C)_{700}AL$.

decreased significantly. This indicates that most of the CuTSPc/C has decomposed and forms the Cu–N–S/C structure, as we observed from the XRD pattern. The differences in the decomposed content of CuTSPc/C between the XPS spectra and the XRD pattern is possibly due to the different measurement techniques, and the encapsulation of the precursor into the carbon frameworks below the detection limit of the XRD analysis. As shown in Fig. 5(b), however, the above Cu2p peaks disappeared totally for the $(CuTSPc/C)_{700}AL$ sample, and no fitting peaks can be achieved, indicating that the metal-Cu is indeed basically removed after the acid-leaching process.

The N1s spectra for both $(CuTSPc/C)_{700}$ and $(CuTSPc/C)_{700}AL$ catalyst samples are presented in Fig. 5(c and d). According to the literature,[37,47,49] the peaks of N1s at 398.6 ± 0.3 eV, 400.5 ± 0.3 eV and 401.3 ± 0.3 eV correspond to pyridinic-N, pyrrolic-N and graphitic-N, where both pyridinic-N and graphitic-N are considered as the active sites for the ORR. As shown in Fig. 5(c),

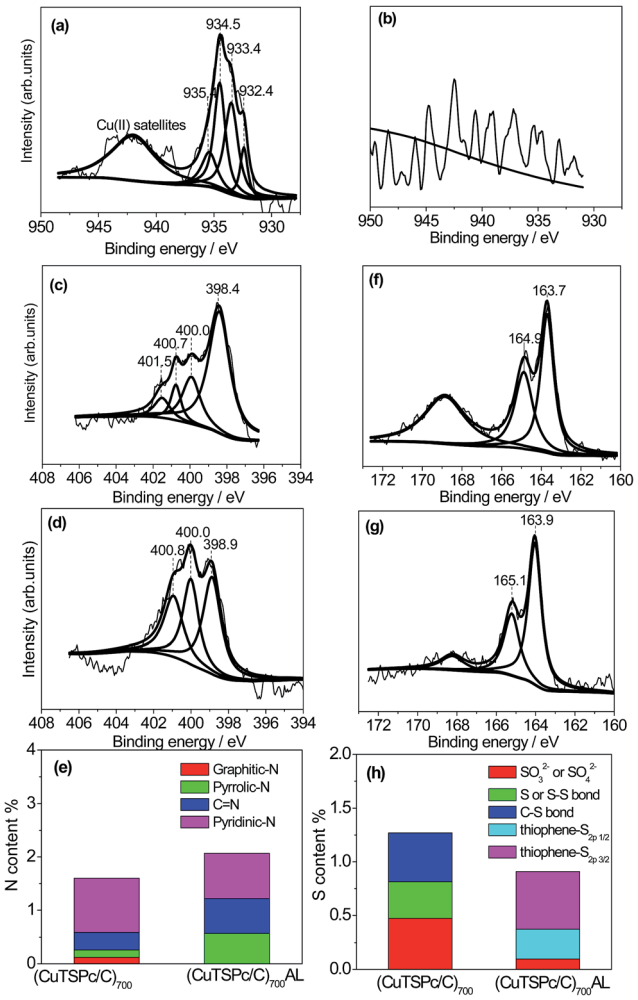

Fig. 5 XPS spectra of (a) Cu2p for $(CuTSPc/C)_{700}$, (b) Cu2p for $(CuTSPc/C)_{700}AL$, (c) N1s for $(CuTSPc/C)_{700}$, (d) N1s for $(CuTSPc/C)_{700}AL$, (e) the content of each type of N for $(CuTSPc/C)_{700}$ and $(CuTSPc/C)_{700}AL$, (f) S2p for $(CuTSPc/C)_{700}$, (g) S2p for $(CuTSPc/C)_{700}AL$, (h) the content of each type of S for $(CuTSPc/C)_{700}$ and $(CuTSPc/C)_{700}AL$.

Table 2 Concentrations (at%) of C, N, O, S and Cu in the $(CuTSPc/C)_{700}$ and $(CuTSPc/C)_{700}AL$ catalyst samples, determined *via* XPS

Sample	C	N	O	S	Cu
$(CuTSPc)_{700}$	88.71	1.60	7.05	1.27	0.38
$(CuTSPc)_{700}AL$	88.63	2.07	8.40	0.91	—

the N1s band for the $(CuTSPc/C)_{700}$ catalyst can be deconvoluted into four peaks with binding energies of 398.4 eV, 400.0 eV, 400.7 eV and 401.5 eV, respectively. The peak at 400.0 eV can be assigned to C=N,[50] while the other three peaks are due to pyridinic-N (398.4 eV), pyrrolic-N (400.7 eV) and graphitic-N (401.5 eV). However, after acid-leaching, only three N1s bands are observed, at 398.9 eV (pyridinic-N), 400.0 eV (C=N) and 400.8 eV (pyrrolic-N), where the graphitic-N totally disappeared, as can be clearly seen in Fig. 5(d). Combined with the results obtained from Fig. 1 and 2, if associating the remarkable ORR activity of the $(CuTSPc/C)_{700}$ catalyst with the observed pyridinic-N peak and graphitic-N peak, one may propose that the active sites for the ORR are essentially weakened due to the loss of Cu during the acid-leaching process.

For a more convenient comparison, the contents of each type of N (the density of active species) are summarized in Fig. 5(e). It is interestingly to find that although the graphitic-N disappeared in the $(CuTSPc/C)_{700}AL$ catalyst, the total concentration of N species increased from 1.60% for $(CuTSPc/C)_{700}$ to 2.07% for $(CuTSPc/C)_{700}AL$ (Table 2). Moreover, the proportion of pyridine-N decreased greatly from 63.1% for $(CuTSPc/C)_{700}$ to 41.1% for $(CuTSPc/C)_{700}AL$, based on the calculation from Fig. 5(e). On the contrary, the proportion of C=N and pyrrolic-N strongly increased, that is, the density of active sites is greatly decreased after acid-leaching. Therefore, it is reasonable to deduce that the disappearance of graphitic-N and the decrease in pyridine-N leads to a significant degradation of the ORR activity on the $(CuTSPc/C)_{700}$ catalyst electrode. The presence of pyridinic-N may be the reason why the $(CuTSPc/C)_{700}AL$ catalyst still maintains certain ORR activity even after acid-leaching. In our previous work, we have also found that the total mass loss of CuTSPc/C and CuPc/C is much smaller than that of H_2Pc/C,[32,33] indicating that Cu species could effectively prevent phthalocyanine from undergoing thermal decomposition, and contribute to a higher nitrogen content which is of benefit for ORR active sites. All these facts suggest that the presence of central metal-Cu is not only essential in the ORR active site structure, but also plays a key role in stabilization of N active species. These conclusions also coincide well with what is observed from the RDE results (Fig. 1).

Fig. 5(f) and (g) present the results obtained for the S2p spectral region for the catalyst samples before and after acid-leaching. It can be seen that the $(CuTSPc/C)_{700}$ catalyst shows a large band ranging from 166.0–172.0 eV, which can be attributed to the formation of a sulfated copper-containing compound.[51] It also exhibits two primary components at 163.7 eV and 164.9 eV, overlapping with each other. The band at 163.7 eV is assigned to the C–S_n–C structure, and the other band at 164.9 eV is close to that of neutral S (164.5) or the S–S bond

(164.6 eV).[33,51] After acid-leaching, the peak intensity at 167.0–170.0 eV was greatly reduced. In the meantime, the peaks at 163.7 eV and 164.9 eV both positively shifted to 163.9 eV and 165.1 eV, indicating some extent of formation of thiophene-S2$p_{3/2}$ and thiophene-S2$p_{1/2}$, respectively.[18,48] In other words, the content of C–S_n–C is decreased due to the loss of Cu, and results in the formation of thiophene-S after the acid-leaching process. Calculated from Fig. 5(h), the proportion of thiophene-S2$p_{1/2}$ structure in the total S for the catalyst is about 30%. Based on these observations, we can infer that the certain extent of decrease in C–S_n–C and the large decrease in active N species can be the reason for the lower ORR activity of the $(CuTSPc/C)_{700}$AL catalyst than that of the $(CuTSPc/C)_{700}$ catalyst. Although the S2$p_{1/2}$ at 165.1 eV is confirmed as the active sulfur component,[18,52] the formation of active thiophene-S2$p_{1/2}$ obviously could not make up for the large decrease in active N species. It is further demonstrated by these facts that the presence of Cu plays a key role in both the formation and stabilization of N active species and active C–S_n–C species.

4. Conclusions

In conclusion, the role of the central metal-Cu ion in the ORR active sites of the CuTSPc/C catalyst was investigated using an acid-leaching model. Through electrochemical measurements and physical characterization analyses, some important results can be obtained: (i) the RDE results show that the acid-leaching process has a negative effect on the ORR activity, where the half-wave potential for the $(CuTSPc/C)_{700}$AL catalyst is negatively shifted by more than 50 mV compared to the $(CuTSPc/C)_{700}$ sample; (ii) the RRDE results indicate that, compared to the $(CuTSPc/C)_{700}$ sample, the ORR path of the $(CuTSPc/C)_{700}$AL catalyst electrode is still a $4e^-$-dominated process, but the electron transfer number obviously decreased, with a greatly increased H_2O_2 yield, particularly in the lower overpotential range; (iii) the XRD and TEM analyses reveal that acid-leaching can remove effectively most of the Cu. The XPS results demonstrate that the central metal-Cu ion not only is an important component for constructing the $(CuTSPc/C)_{700}$ catalyst ORR active sites, but also has a great effect on the stability of the active N and S species.

Acknowledgements

The authors gratefully acknowledge financial support from the National Natural Science Foundation of China (21173039); International Academic Cooperation and Exchange Program of Shanghai Science and Technology Committee (14520721900); the Specialized Research Fund for the Doctoral Program of Higher Education, SRFD (20110075110001) of China, and College of Environmental Science and Engineering, State Environmental Protection Engineering Center for Pollution Treatment and Control in Textile Industry, Donghua University, Shanghai 201620, China. All the financial support is gratefully acknowledged.

References

1 S. Srinivasan, *Fuel cells: from fundamentals to applications*, New York, Springer, 2006.
2 G. Hooger, *Fuel cell technology handbook*, Boca Raton, CRC Press, 2002.
3 J. F. Wu, X. Z. Yuan, J. J. Martina, H. J. Wang, J. J. Zhang, J. Shen, S. H. Wu and W. Merid, A review of PEM fuel cell durability: degradation mechanisms and mitigation strategies, *J. Power Sources*, 2008, **184**, 104–119.
4 M. P. Hogarth and T. R. Ralph, Catalysis for low temperature fuel cells, *Platinum Met. Rev.*, 2002, **46**, 146–164.
5 M. M. Mench, C. Y. Wang and S. T. Thynell, An introduction to fuel cells and related transport phenomena, *Int. J. Transp. Phenom.*, 2001, **3**, 151–176.
6 F. Gloaguen, P. Convert, S. Gamburzev, O. A. Velev and S. Srinivasan, An evaluation of the macro-homogeneous and agglomerate model for oxygen reduction in PEMFCs, *Electrochim. Acta*, 1998, **43**, 3767–3772.
7 M. M. Matthew, C. Y. Wang and T. T. Stefan, A review of polymer electrolyte membrane fuel cells: technology, applications, and needs on fundamental research, *Appl. Energy*, 2011, **88**, 981–1007.
8 Y. W. Ou, H. Kumagai, F. X. Yin, S. Okada, H. Hatasawa, H. Morioka, K. Takanabe, J. Kubota and K. Domen, Electrocatalytic Activity and Stability of M-Fe Catalysts Synthesized by Polymer Complex Method for PEFC Cathode, *J. Electrochem. Soc.*, 2011, **158**, B1491–B1498.
9 J. H. Kim, I. Akimitsu, M. Shigenori, K. Nobuyuki and K. I. Ota, Catalytic activity of titanium oxide for oxygen reduction reaction as a non-platinum catalyst for PEFC, *Electrochim. Acta*, 2007, **52**, 2492–2497.
10 B. Wang, Recent development of non-platinum catalysts for oxygen reduction reaction, *J. Power Sources*, 2005, **152**, 1–15.
11 J. L. Qiao, L. Xu, Y. Y. Liu, P. Xu, J. J. Shi, S. Y. Liu and B. L. Tian, Carbon-supported co-pyridine as non-platinum cathode catalyst for alkaline membrane fuel cells, *Electrochim. Acta*, 2013, **96**, 298–305.
12 E. M. Sommer, L. S. Martins, J. V. C. Vargas, J. E. F. C. Gardolinski, J. C. Ordonez and C. E. B. Marino, Alkaline membrane fuel cell (AMFC) modeling and experimental validation, *J. Power Sources*, 2012, **2**, 16–30.
13 E. Gülzow, Alkaline fuel cells: a critical view, *J. Power Sources*, 1996, **61**, 99–104.
14 Z. W. Chen, H. Drew, A. P. Yu, L. Zhang and J. J. Zhang, A review on non-precious metal electrocatalysts for PEM fuel cells, *Energy Environ. Sci.*, 2011, **4**, 3167–3192.
15 X. G. Li, C. P. Liu, W. Xing and T. H. Lu, Development of durable carbon black/titanium dioxide supported macrocycle catalysts for oxygen reduction reaction, *J. Power Sources*, 2009, **193**, 470–476.
16 P. S. Nalini, X. G. Li, N. Vijayadurda, P. K. Swaminatha, C. M. Hector, G. Wu, J. W. Lee and N. P. Branko, Nitrogen-modified carbon-based catalysts for oxygen reduction reaction in polymer electrolyte membrane fuel cells, *J. Power Sources*, 2009, **188**, 38–44.

17 A. Morozan, B. Jousselme and S. Palacin, Low-platinum and platinum-free catalysts for the oxygen reduction reaction at fuel cell cathodes, *Energy Environ. Sci.*, 2011, **4**, 1238–1254.

18 J. J. Shi, X. J. Zhou, P. Xu, J. L. Qiao, Z. W. Chen and Y. Y. Liu, Nitrogen and Sulfur Co-doped Mesoporous Carbon Materials as Highly Efficient Electrocatalysts for Oxygen Reduction Reaction, *Electrochim. Acta*, 2014, **145**, 259–269.

19 W. B. Cicero, L. Zhang, K. Lee, H. S. Liu, L. B. M. Aldalea, P. M. Edmar, H. J. Wang and J. J. Zhang, A review of Fe–N/C and Co–N/C catalysts for the oxygen reduction reaction, *Electrochim. Acta*, 2008, **53**, 4937–4951.

20 J. L. Qiao, L. Xu, L. Ding, L. Zhang, R. Baker, X. F. Dai and J. J. Zhang, Using pyridine as nitrogen-rich precursor to synthesize Co–N–S/C non-noble metal electrocatalysts for oxygen reduction reaction, *Appl. Catal., B*, 2012, **125**, 197–205.

21 I. Kruusenberg, L. Matisen and K. Tammeveski, Oxygen electroreduction on multi-walled carbon nanotube supported metal phthalocyanines and porphyrins in alkaline media, *J. Nanosci. Nanotechnol.*, 2013, **13**, 621–627.

22 L. Ding, X. Qing, X. J. Zhou, J. L. Qiao, H. Li and H. J. Wang, Electrochemical behavior of nanostructured nickel phthalocyanine (NiPc/C) for oxygen reduction reaction in alkaline media, *J. Appl. Electrochem.*, 2013, **43**, 43–51.

23 G. Wu, L. Karren, M. J. Christina and Z. Piotr, High-performance electrocatalysts for oxygen reduction derived from polyaniline, iron and cobalt, *Science*, 2011, **332**, 443–447.

24 L. Ding, X. F. Dai, R. Lin, H. J. Wang and J. L. Qiao, Electrochemical performance of carbon-supported Co-phthalocyanine modified with Co-added metals (M = Fe, Co, Ni, V) for oxygen reduction reaction, *J. Electrochem. Soc.*, 2012, **159**, F577–F584.

25 U. I. Kramm, I. Abs-Wurmbach, I. Herrmann-Geppert, J. Radnik, S. Fiechter and P. Bogdanoff, Influence of the electron-density of FeN_4-centers towards the catalytic activity of pyrolyzed FeTMPPCl-based ORR-electrocatalysts, *J. Electrochem. Soc.*, 2011, **158**, B69–B78.

26 P. Xu, W. Z. Chen, Q. Wang, T. S. Zhu, M. J. Wu, J. L. Qiao, Z. W. Chen and J. J. Zhang, Effects of transition metal precursors (Co, Fe, Cu, Mn, or Ni) on pyrolyzed carbon supported metal-aminopyrine electrocatalysts for oxygen reduction reaction, *RSC Adv.*, 2015, **5**, 6195–6206.

27 Y. Nabae, S. Moriya, K. Matsubayashi, S. M. Lyth, M. Malon, L. B. Wu, N. MIslam, Y. Koshigoe, S. Kuroki, M. AKakimoto, S. Miyata and J. Ozaki, The role of Fe species in the pyrolysis of Fe phthalocyanine and phenolic resin for preparation of carbon-based cathode catalysts, *Carbon*, 2010, **48**, 2613–2624.

28 R. P. Baker, D. Wilkinson and J. J. Zhang, Electrocatalytic activity and stability of substituted iron phthalocyanines towards oxygen reduction evaluated at different temperatures, *Electrochim. Acta*, 2008, **53**, 6906–6919.

29 I. Kruusenberg, L. Matisen, Q. Shah, A. M. Kannan and K. Tammeveski, Non-platinum cathode catalysts for alkaline membrane fuel cells, *Int. J. Hydrogen Energy*, 2012, **37**, 4406–4412.

30 Z. P. Li and B. H. Liu, The use of macrocyclic compounds as electrocatalysts in fuel cells, *J. Appl. Electrochem.*, 2010, **40**, 475–483.

31 N. Sehlotho and T. Nyokong, Effects of ring substituents on electrocatalytic activity of manganese phthalocyanines towards the reduction of molecular oxygen, *J. Electroanal. Chem.*, 2006, **595**, 161–167.

32 L. Ding, J. L. Qiao, X. F. Dai, J. Zhang, J. J. Zhang and B. L. Tian, Highly active electrocatalysts for oxygen reduction from carbon-supported copper-phthalocyanine synthesized by high temperature treatment, *Int. J. Hydrogen Energy*, 2012, **37**, 14103–14113.

33 X. Qing, J. J. Shi, C. Y. Ma, M. Y. Fan, Z. Y. Bai, Z. W. Chen, J. L. Qiao and J. J. Zhang, Simultaneous formation of nitrogen and sulfur-doped transition metal catalysts for oxygen reduction reaction through pyrolyzing carbon-supported copper phthalocyanine tetrasulfonic acid tetrasodium salt, *J. Power Sources*, 2014, **266**, 88–98.

34 L. Qu, Y. Liu, J. B. Baek and L. M. Dai, Nitrogen-doped graphene as efficient metal-free electrocatalyst for oxygen reduction in fuel cells, *ACS Nano*, 2010, **4**, 1321–1326.

35 L. P. Zhang, J. B. Niu, L. M. Dai and Z. H. Xia, Effect of microstructure of nitrogen-doped graphene on oxygen reduction activity in fuel cells, *Langmuir*, 2012, **28**, 7542–7550.

36 W. Xia, J. Masa, M. Bron, W. Schuhmann and M. Muhler, Highly active metal-free nitrogen-containing carbon catalysts for oxygen reduction synthesized by thermal treatment of polypyridine–carbon black mixtures, *Electrochem. Commun.*, 2011, **13**(6), 593–596.

37 X. G. Li, B. N. Popova, T. Kawaharab and H. Yanagi, Non-precious metal catalysts synthesized from precursors of carbon, nitrogen, and transition metal for oxygen reduction in alkaline fuel cells, *J. Power Sources*, 2011, **196**, 1717–1722.

38 J. J. Shi, X. J. Zhou, P. Xu, J. L. Qiao, Z. W. Chen and Y. Y. Liu, Nitrogen and Sulfur Co-doped Mesoporous Carbon Materials as Highly Efficient Electrocatalysts for Oxygen Reduction Reaction, *Electrochim. Acta*, 2014, **145**, 259–269.

39 P. Justin, P. H. K. Charan and G. R. Rao, Activated zirconium carbide promoted Pt/C electrocatalyst for oxygen reduction, *Appl. Catal., B*, 2014, **144**, 767–774.

40 Y. J. Hu, H. Zhang, P. Wu, H. Zhang, B. Zhou and C. X. Cai, Bimetallic Pt–Au nanocatalysts electrochemically deposited on graphene and their electrocatalytic characteristics towards oxygen reduction and methanol oxidation, *Phys. Chem. Chem. Phys.*, 2011, **13**, 4083–4094.

41 Q. Y. Liu, Z. Y. Liu, Z. P. Zhu, G. Y. Xie and Y. L. Wang, Al_2O_3-coated honeycomb cordierite-supported CuO for simultaneous SO_2 and NO removal from flue gas: effect of Na_2O additive, *Ind. Eng. Chem. Res.*, 2004, **43**, 4031–4037.

42 X. G. Wen, W. X. Zhang, S. H. Yang, Z. R. Dai and Z. L. Wang, Solution phase synthesis of $Cu(OH)_2$ nanoribbon by coordination self-assembly using Cu_2S nanowires as precursors, *Nano Lett.*, 2002, **2**, 1397–1401.

43 K. Xiao, R. J. Li, J. Tao, E. A. Payzant, I. N. Ivanov, A. A. Puretzky, W. P. Hu and D. B. Geohegan, Metastable

copper-phthalocyanine single-crystal nanowires and their use in fabricating high-performance field-effect transistors, *Adv. Funct. Mater.*, 2009, **19**, 3776–3780.

44 G. Soto, J. A. Díaz and W. D. L. Cruz, Copper nitride films produced by reactive pulsed laser deposition, *Mater. Lett.*, 2003, **57**, 4130–4133.

45 S. Velu, K. Suzuki, M. Vijayaraj, S. Barman and C. S. Gopinath, *In situ* XPS investigations of $Cu_{1-x}Ni_xZnAl$-mixed metal oxide catalysts used in the oxidative steam reforming of bio-ethanol, *Appl. Catal., B*, 2005, **55**, 287–299.

46 T. B. Du, Y. Luo and V. Desai, The combinatorial effect of complexing agent and inhibitor on chemical-mechanical planarization of copper, *Microelectron. Eng.*, 2004, **71**, 90–97.

47 S. L. Gojkovic, S. Gupta and R. F. Savinell, Heat-treated iron(III) tetramethoxyphenyl porphyrin chloride supported on high-area carbon as an electrocatalyst for oxygen reduction Part II. Kinetics of oxygen reduction, *J. Electroanal. Chem.*, 1999, **462**, 63–72.

48 Q. G. He, X. F. Yang, R. H. He, B. L. Agustín, M. Hamish, X. M. Ren, W. L. Yang and K. E. Bruce, Electrochemical and spectroscopic study of novel Cu and Fe-based catalysts for oxygen reduction in alkaline media, *J. Power Sources*, 2012, **213**, 169–179.

49 K. C. Lee, L. Zhang, H. S. Liu, R. Hui, Z. Shi and J. J. Zhang, Oxygen reduction reaction (ORR) catalyzed by carbon-supported cobalt polypyrrole (Co-PPy/C) electrocatalysts, *Electrochim. Acta*, 2009, **54**, 4704–4711.

50 V. Nallathambi, J. W. Lee, S. P. Kumaraguru, G. Wu and B. N. Popov, Development of high performance carbon composite catalyst for oxygen reduction reaction in PEM proton exchange membrane fuel cells, *J. Power Sources*, 2008, **183**, 34–42.

51 H. Gao, Z. Liu, L. Song, W. H. Guo, W. Gao, L. J. Ci, A. Rao, W. J. Quan, R. Vajtai and P. M. Ajayan, Synthesis of S-doped graphene by liquid precursor, *Nanotechnology*, 2012, **23**, 1–7.

52 Z. Liu, H. G. Nie, Z. Yang, J. Zhang, Z. P. Jin, Y. Q. Lu, Z. B. Xiao and M. H. Shao, Sulfur-nitrogen co-doped three-dimensional carbon foams with hierarchical pore structures as efficient metal-free electrocatalysts for oxygen reduction reactions, *Nanoscale*, 2013, **5**, 3283–3288.

